JOURNAL OF SOLID STATE CHEMISTRY **121,** 202–213 (1996)
ARTICLE NO. 0029

Structural, Magnetic, and Thermal Properties of $La_{1-t}Ca_tCrO_{3-\delta}$

Natsuko Sakai,*[,1] Helmer Fjellvåg,* and Bjørn C. Hauback†

*Department of Chemistry, University of Oslo, N-0315 Oslo, Norway; and †Institutt for energiteknikk, N-2007 Kjeller, Norway

Received April 14, 1995; in revised form September 18, 1995; accepted September 19, 1995

A broad study on the properties of Ca-substituted $LaCrO_3$ is reported. Problems in the synthesis of Ca-rich samples of $La_{1-t}Ca_tCrO_{3-\delta}$ are addressed. For the La-rich region, synthesis in air provides $La_{1-t}Ca_tCrO_3$ with partial formation of Cr^{IV}. At reducing conditions, Cr^{IV} can be converted to Cr^{III}. The properties of oxidized and reduced samples are compared since differences are of importance for applications. The maximum reduction, without decomposition, corresponds ideally to $\delta = t/2$, but this could not be fully achieved in 10% H_2 + 90% N_2 at 1263 K. Unit cell data, atomic coordinates (from powder neutron diffraction data), thermal expansion, and magnetic property data are provided. The crystal structure is orthorhombic ($GdFeO_3$-type) at 298 K; the rhomobohedral $LaAlO_3$-type variant exists at high temperatures. Sample reduction influences slightly the orthorhombic distortion, increases the unit cell volume quite considerably, enhances the temperature domain of the orthorhombic versus the rhombohedral modification, and increases the magnetic moment and the antiferromagnetic ordering temperature. The microscopic thermal expansion is independent of the Ca content ($0.00 \leq t \leq 0.30$) and is slightly enhanced for the rhombohedral phase. The antiferromagnetic G_x-type ordering in $LaCrO_3$ is retained upon substitution. However, for oxidized samples, a smaller A_z component develops upon substitution, whereas for field cooled samples parasitic ferromagnetism appears. For fully reduced samples, the aliovalent Ca substitution implies unit cell compression and oxygen vacancy formation with modest effect on magnetic properties. The additional partial exchange of Cr^{III} (d^3) by Cr^{IV} (d^2) for oxidized samples has significant impact on the magnetic properties.

1. INTRODUCTION

Alkaline earth substituted lanthanum chromites, $La_{1-t}M_tCr_{1-z}T_zO_{3-\delta}$ (M = Ca, Sr, and T = Mg) have obtained a large interest during the past decades due to possible technological use of such materials as electrodes in magnetohydrodynamic generators (1) or as interconnects in solid oxide fuel cells (2–5). The materials take the perovskite-type structure and have high electronic conductivities at high temperatures. Lanthanum chromite itself, $LaCrO_3$, is well known to exhibit high chemical stability over a wide range of temperatures and oxygen partial pressures. Studies on the defect chemistry of substituted and nonstoichiometric lanthanum chromites have been done by electrical conductivity (6), Seebeck coefficient (7, 8), and thermogravimetric (9, 10) measurements. When some La^{III} is substitutionally exchanged by aliovalent M^{II} (at the A-site), the decrease in positive charge can be compensated either by valence change of chromium or by formation of oxygen vacancies. Both scenarios, depending on temperature (T)–oxygen partial pressure [$p(O_2)$] conditions, are realized.

In the higher $p(O_2)$ range, e.g., in air, the oxygen deficit (δ) for the partly substituted $La_{1-t}Ca_tCrO_{3-\delta}$ is close to zero. The charge compensation occurs via valence change of Cr, with resulting substantial electronic conductivity (p-type). In Kröger–Vink notation the substitution is described as

$$MCrO_3 \rightarrow M'_{La} + Cr^{\cdot}_{Cr} + 3O^{x}_{O} \text{ in } LaCrO_3, \qquad [1]$$

whereas in the low $p(O_2)$ range, the compensation is achieved by formation of oxygen vacancies, and the electrical transport is more ionic in nature. Formally, the situation can be considered as a reduction of the four valent Cr (formed according to [1]),

$$2Cr^{\cdot}_{Cr} + O^{x}_{O} \rightarrow 2Cr^{x}_{Cr} + V^{\cdot\cdot}_{O} + 1/2\ O_2(g). \qquad [2]$$

The properties of alkaline earth substituted $LaCrO_3$ have been the subject for a large number of studies, in particular for M = Ca and Sr (11, 12), where mainly the T, $p(O_2)$ dependences of defect-related properties such as electronic conductivity (6, 13), ionic transport (14), and sinterability (15, 16) have been considered. For both substituents, a shrinkage of the unit cell is observed, however, details for the atomic arrangement as functions of composition and temperature are not available.

The present paper aims at clarifying composition induced changes in the atomic arrangement, thermal expan-

[1]Permanent address: Department of Inorganic Materials, National Institute of Materials and Chemical Research, 1-1 Higashi, Tsukuba, Ibaraki 305, Japan.

0022-4596/96 $12.00

sion, phase transition features, and magnetic order of $La_{1-t}Ca_tCrO_{3-\delta}$. Samples with different oxygen stoichiometries are obtained by selecting proper temperature and oxygen partial pressure conditions during the final heating. In this way the average oxidation state of Cr is monitored. Data are provided for oxidized ($\delta \approx 0.00$) and reduced ($0 < \delta \leq t/2$) samples. The change in properties between samples with the two extreme compositions ($\delta = 0$ and $\delta = t/2$) is highly relevant for the potential use of such materials as interconnects in solid oxide fuel cells. In particular, composition induced changes in the thermal expansitivity as well as in the volume jump of the first-order transition between orthorhombic ($GdFeO_3$-type) and rhombohedral ($LaAlO_3$-type) modifications are described.

Data for hydrothermally synthesized $La_{1-t}Ca_tCrO_3$ indicate that the antiferromagnetic ordering temperature ($T_N \approx 290$ K) is independent of the substitution level (17). However, the exact oxygen stoichiometry of these samples, which for sure were partly reduced, can be questioned. The present study provides magnetization data for oxidized and reduced samples (with varying Cr^{III}/Cr^{IV} ratio). Furthermore, details on the magnetic structure are provided on the basis of powder neutron diffraction data.

2. EXPERIMENTAL

Samples of $La_{1-t}Ca_tCrO_{3-\delta}$ ($t = 0.00, 0.10, 0.20$, and 0.30) were prepared according to a modified Pechini method (18). Appropriate amounts of La_2O_3 (99.99%), $CaCO_3$ (98%), and $Cr(NO_3)_3$ (98%), all guaranteed reagents, Nakarai Chemical Co. Ltd., Japan, were dissolved in diluted HNO_3. Thereafter, an excess of citric acid was added to the solution. After complete dissolution of the citric acid, the solution was heated on a hot plate to remove water and nitric oxides, and the liquid turned eventually into a glassy gel. The gel was dried at 460 K, and then crushed and thoroughly mixed in ethanol in a ZrO_2 ball mill (6 hr). After removal of the ethanol, the powder was calcined at 1473 K for 10 hr in air. For the highest Ca contents $t = 0.50$ and 0.75, La_2O_3 (99.99% Molycorp. Inc.), $CaCO_3$ (>99%, Merck), and CrO_3 (>99%, Fluka) were used as starting materials. The preparation procedure followed mostly that described for $0.00 \leq t \leq 0.30$, however, drying at 460 K and mixing in ethanol were omitted. After the gel was dried on a hot plate, the sample was immediately calcined at 1873 K in air for 5 hr. Reduced samples of $La_{1-t}Ca_tCrO_{3-\delta}$, $t = 0.10$ and 0.20, were obtained by treatment in 10% H_2 + 90% N_2, and for $t = 0.30$, 0.50, and 0.75 in CO/CO_2 mixtures. The samples were heated to 1173–1273 K and then cooled to room temperature. The reducing gas mixture was kept during the entire treatment. The temperature and the CO/CO_2 mixing ratio were regulated for each sample during the annealing step prior to cooling in order to obtain the most suitable reducing conditions without any accompanying decomposition. For example, $La_{0.70}Ca_{0.30}CrO_3$ was reduced at $T = 1173$ K in a $CO:CO_2 = 83:17$ gas mixture resulting in an oxygen content of $3 - \delta = 2.88$ for the single phase product. The oxygen contents of the reduced samples were estimated from the weight increase during reoxidation in a Perkin Elmer TGA7.

All samples were characterized by powder X-ray diffraction (PXD) at room temperature [Guinier–Hägg cameras, $CuK\alpha_1$ radiation, Si as internal standard; $a = 543.1065$ pm (19)] in order to determine phase purity and sample homogeneity. No reflections from additional phases were observed for samples with $t \leq 0.50$. For $t = 0.75$, small amounts of CaO and β-$CaCr_2O_4$ were observed. Unit cell dimensions were determined by least square methods from data for about 15 Bragg reflections using the UNITCELL program (20). As an aid in correct indexing of reflections for the orthorhombic unit cell with pseudocubic metric, calculated PXD patterns were obtained with the LAZY PULVERIX program (21).

High-temperature powder X-ray diffraction data were collected in two ways. First, a Guinier Simon camera (Enraf Nonius) was used for temperatures between 300 and 1200 K ($t = 0.20$, $\delta = 0.00$ and 0.10). The samples were contained in rotating, sealed or open, quartz capillaries, and the programmed temperature change was synchronized with the movement of the film casette. The temperature was calibrated by means of measurements of the known volume expansion of silver (22). In accordance with data for $La_{0.7}Sr_{0.3}CrO_3$ in Ref. (9) and own TGA data, the oxidized samples did not loose oxygen at temperatures below 1200 K. Therefore the stoichiometry of the oxidized samples were retained during the PXD studies. The reduced samples were kept within closed capillaries during the experiments which prevented overall compositional changes, although decomposition may occur. Second, a Macρ diffractometer (Mac Science Ltd., Japan) was used. A dense polycrystalline disk (8-mm diameter and 1-mm thick) was placed in a platinum holder and corrections were made for settling the correct average height of the sample surface. A Pt–Pt 13% Rh thermocouple was attached to the sample to monitor the temperature. Dried air (20% O_2 and 80% N_2, from gas cylinder) flowed through the sample chamber during the high temperature experiments (30 ml/min).

Powder neutron diffraction (PND) data were collected on the OPUS IV two-axis diffractometer at the JEEP II reactor, Kjeller, at and below room temperature. Cylindrical sample holders were used. Monochromatized neutrons of wavelength 182.5 pm were obtained by reflection from Ge(111). The diffraction patterns were measured by means of five ^{3}He detectors, positioned 10° apart. Intensity data were collected from $2\Theta = 15°$ to 100° in steps of $\Delta 2\Theta = 0.05°$. A typical data set contained 1700 measuring points,

and some 80 reflections entered into the profile refinements (see below). Temperatures between 10 and 300 K were obtained by means of a Displex cooling system. A Lake Shore DRC 82C controller was used, and the temperature was measured and controlled by means of a silicon diode.

A second set of PND data were collected at the University of Missouri Research Reactor (MURR) using the PSD II two-axis diffractometer. The 511 reflection from a bent, cylindrical, perfect Si crystal gave monochromatic neutrons of wavelength 147.66 pm. Intensities were measured by an array of five 600 mm position sensitive ^{3}He detectors (PSD), covering 20° in 2Θ (23). A complete diagram, from 2Θ = 5° to 105°, was obtained by moving the detector unit in five steps. The collected data were converted to 2Θ values in steps of Δ2Θ = 0.05°. A typical data set contained 2000 measuring points, and some 165 reflections entered into the profile refinements.

Structural and instrumental parameters were obtained from profile refinements. The Hewat version of the Rietveld program (24, 25) was used, and the results were compared with similarly refined data using the ALLHKL and EDINP programs (26, 27). One scale factor, three half width parameters, three unit cell dimensions, zero point, and seven positional parameters together with four isotropic displacement factors entered into the least square refinements. The scattering amplitudes $b_{La} = 8.24$, $b_{Ca} = 4.70$, $b_{Cr} = 3.635$, and $b_O = 5.805$ fm (28) were adopted. For the low temperature data, three additional parameters entered for description of the magnetic structures. The form factors for Cr^{3+} from Ref. (29) were used.

Magnetization data were measured by a SQUID magnetometer (MPMS; Quantum Design) between 5 and 300 K. Data were collected for zero field cooled (ZFC) samples on heating in a field of 100 Oe. Furthermore, data were collected on cooling (FC) in a field of 1 kOe. Magnetization data in high fields, $H \leq 50$ kOe, were collected at 5 K.

3. RESULTS AND DISCUSSION

3.1. Synthesis and Solid Solubility for $La_{1-t}Ca_tCrO_{3-\delta}$

$LaCrO_3$, $CaCrO_3$, and $Ca_2Cr_2O_5$ are all end phases for the $La_{1-t}Ca_tCrO_{3-\delta}$ solid solution. Among these phases, $LaCrO_3$ is thermally the most stable, melting at 2783 ± 20 K (30). Berjoan *et al.* (11) claimed increased stability for samples with around 8% calcium at the A site of the solid solution phase. The Ca-end phases can only be obtained with more difficulty. $CaCrO_3$, with solely Cr^{IV}, requires high pressure techniques (31), whereas $Ca_2Cr_2O_5$ has first recently been synthesized and has apparently a maximum thermal stability of around 1300 K (32). In the La–Ca–Cr–O system, a region of partial melting exists in the Ca-rich part, which prevents the use of high temperatures in the synthesis (11). In addition, earlier investigations have encountered problems due to phase splitting for $t \geq 0.30$ into oxygen rich and oxygen poor solid solution phases (17) and demixing of the solid solution phase at certain conditions (33, 34). The introduction of calcium into the stable $LaCrO_3$ phase is probably best done via mixing at an atomic level in a precursor phase, presently in citrate gels.

During the incineration of the precursor in oxygen rich atmospheres, high valent Cr phases like $CaCrO_4$, $LaCrO_4$, La_2CrO_6, and $Ca_3(CrO_4)_2$ were found as intermediates, which partly caused inhomogeneous products during the subsequent thermal decomposition and sintering reaction. Phase pure sample of $La_{1-t}Ca_tCrO_3$, $0.00 \leq t \leq 0.30$, were obtained after a second heating in air at 1473 K. The distribution of Ca and La over the A site is random, as indicated by small half-widths of the Bragg reflections and lacking superstructure reflections. This was separately confirmed in the PND study (see below).

For the $La_{0.25}Ca_{0.75}CrO_{3-\delta}$ sample, impurities of CaO and β-$CaCr_2O_4$ were present, even after the second heat treatment. This is probably not directly caused by the formation of the various intermediates during the heating, but reflects instead the minor stability of the solid solution phase with respect to neighboring phases. At lower temperatures (e.g., 1300 K), $CaCrO_4$ with hexavalent chromium is easily formed, whereas the products change into CaO and β-$CaCr_2O_4$ if higher reaction temperatures are operative. No further attempts were made to search for optimal synthesis conditions (temperature and atmosphere). In the presently adopted CO/CO_2 atmosphere with $p(O_2) \approx 10^{-11}$ Pa, decomposition does notably not take place at 1173 K; there is only partial reduction. At high oxygen partial pressures, the stability of the phase extends at least up to 1800 K, whereas at strongly reducing conditions (H_2/N_2) decomposition into CaO, $CaCr_2O_4$, and $La_{1-t}Ca_tCrO_{3-\delta}$ with a lower Ca-content occurs around 1300 K. The variation of the unit cell dimensions with composition (Table 1 and Fig. 1) suggests clearly that complete solid solubility may exist. For the oxygen saturated samples ($\delta = 0.00$), a smooth variation of the unit cell volume is observed. However, the slight positive deviation from a Vegard law relationship for the solid solution phase may either indicate increasing noncomplete oxidation for heavily substituted samples, which is reasonable since high pressure methods are required for, e.g., $CaCrO_3$ (31), and/or indicate repulsive La–Ca interactions which possibly may explain the observed tendency toward demixing, which in this case, should be enhanced if the annealing temperature is lowered. The latter hypothesis is consistent with the observations by Carter *et al.* (34) who reported that the solid solution phase exists only at high temperatures and that an immiscibility domain opens at lower temperatures. For the reduced samples, the unit cell volume is much lower than expected for $t = 0.50$ and 0.75 (Fig. 1). This may either indicate incomplete reduction at the applied conditions or a rapid reoxidation prior to the PXD studies. A different,

TABLE 1

Unit Cell Dimensions and Axial Ratios for $La_{1-t}Ca_tCrO_{3-\delta}$ Obtained from PXD Data (Guinier–Hägg Technique; Oxidized and Reduced Samples)

t	a (pm)	b (pm)	c (pm)	V (10^6 pm^3)
		Oxidized		
0.00	547.90(14)	775.62(14)	551.61(5)	234.41(5)
0.10	546.98(4)	774.25(6)	549.38(5)	232.55(6)
0.20	544.62(4)	772.61(6)	547.44(6)	230.35(3)
0.30	543.68(7)	769.19(9)	545.03(6)	228.04(5)
0.50	540.37(6)	764.63(9)	541.18(5)	223.61(4)
0.75[a]	537.30(20)	754.21(118)	538.68(30)	218.39(39)
		Reduced		
0.10	547.19(8)	775.05(18)	550.80(8)	233.59(7)
0.20	545.54(11)	774.74(22)	549.87(9)	232.41(9)
0.30	545.19(8)	774.12(11)	548.14(7)	231.34(6)
0.50	543.68(22)	768.83(12)	544.08(5)	227.42(10)
0.75*	540.00(7)	764.04(14)	540.55(4)	223.02(4)

Note. Space group *Pnma*. Calculated standard deviations in parentheses.

[a] Impurities present.

but also possible explanation, is that an additional volume expansion occurs for the highly ordered defects in $Ca_2Cr_2O_5$. However, this is not plausible since the volume difference between samples with $\delta = 0.00$ and $\delta = t/2$ (for $t = 1.00$) corresponds nicely to what was expected from the size difference between Cr^{III} and Cr^{IV} in binary chromium oxides (35).

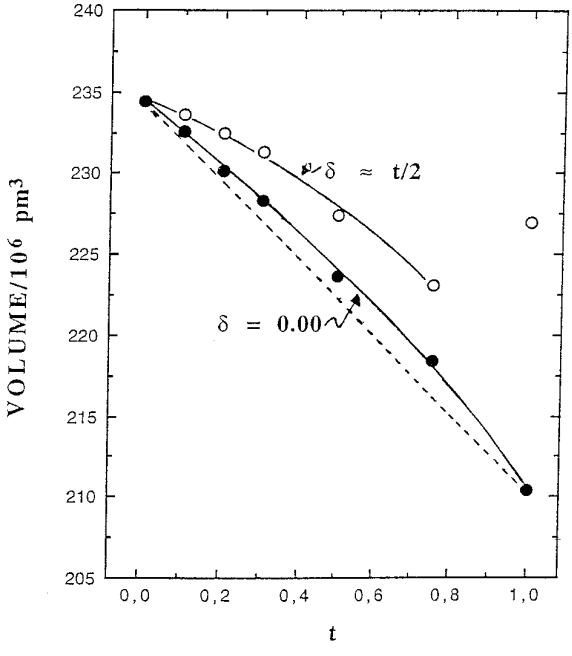

FIG. 1. Unit cell volume at 298 K for oxidized and reduced samples of $La_{1-t}Ca_tCrO_{3-\delta}$. Calculated standard deviations do not exceed size of symbol. Fully drawn lines guide the eye, dotted line shows Vegard law relationship.

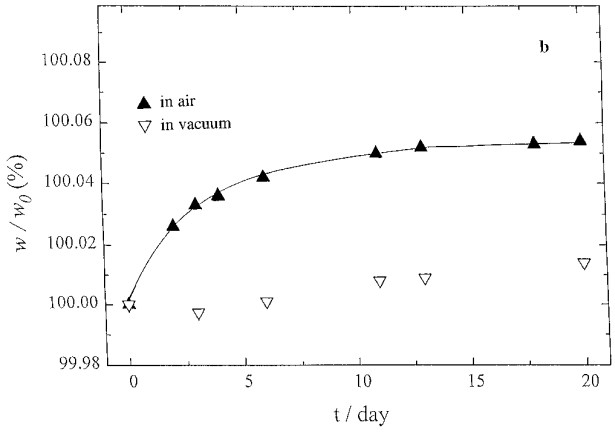

FIG. 2. Termogravimetric curve showing reoxidation of $La_{0.80}Ca_{0.20}CrO_{3-\delta}$ on long time exposure to air and vacuum conditions at 298 K. Fully drawn line guides the eye.

The reduced $La_{1-t}Ca_tCrO_{3-\delta}$ are susceptible for reoxidation into $La_{1-t}Ca_tCrO_3$. The reductions and oxidations represent topotactic reactions. In related phases, such as $LaCoO_{3-\delta}$, reduction at low temperatures gives a metastable, highly defective perovskite rather than forcing a phase separation into the stable two-phase mixture of La_2CoO_4 and CoO (36). It is not clear whether reduced $La_{1-t}Ca_tCrO_{3-\delta}$ represents the thermodynamically stable situation at the selected conditions. The reoxidizations are slow at room temperature, but do progress. For $t = 0.20$ (partly reduced), the weight increase was registered daily, and during 15 days a 0.05% weight increase caused a change in oxygen stoichiometry ($3 - \delta$) from 2.93 to 2.95 (Fig. 2). Among the samples $0.00 \leq t \leq 0.30$, those with a lower Ca content show the strongest tendency toward rapid reoxidation. TGA data (powder samples; a few μm particle size) shows a more or less well developed two-stage reoxidation behavior in flowing oxygen (onset around 400 K). The stepwise oxidation may indicate enhanced stability of intermediate compositions, reflect diffusion features, or reoxidation of segregated phases (not detectable by PXD).

3.2. Unit Cell, Structural Phase Transition, and Thermal Expansion

The orthorhombic distortions for the unit cell of $La_{1-t}Ca_tCrO_{3-\delta}$ (unit cell dimensions are given in Table 1) are small and can be described in terms of deviations in $(a/c - 1)$ and $(b/c - \sqrt{2})$ from zero. The $GdFeO_3$-type unit cell is related to the cubic unit cell by $\mathbf{a}_o = \mathbf{a}_c - \mathbf{b}_c$, $\mathbf{b}_o = 2\mathbf{c}_c$ and $\mathbf{c}_o = \mathbf{a}_c + \mathbf{b}_c$, subscripts o and c referring to orthorhombic and cubic unit cells, respectively. For both oxidized and reduced samples, the pseudocubic ratios are more closely approached on Ca substitution (see Section

3.3. and Table 1). For the La-rich solid solution, the created oxygen vacancies are probably confined to small defect clusters, e.g., Ca^{2+}–V_O–Ca^{2+} (37). The end member of the reduced solid solution, $Ca_2Cr_2O_5$, has been suggested to take the Brownmillerite- (BR) type structure (33, 38) which, if correct, would imply that on increasing Ca content and vacancy concentration, half of the defect octahedra will finally turn into tetrahedra. For the Brownmillerite-type structure, alternating sheets of octahedra and tetrahedra exist along **b** (Fig. 3) and large deviations in the corresponding axial ratios develop (a_{BR}/c_{BR} and $b_{BR}/2c_{BR}$ being, 1.05 and 1.31, respectively). Also some TEM data are in this respect available for the $La_{1-t}Ca_tCrO_{3-\delta}$ system (39). Presently, no additional peaks in the PXD patterns could give support to superstructure formation for Ca-rich samples.

Visual inspection of the Guinier Simon high-temperature PXD photographs clearly show that the orthorhombic line splittings diminish continuously on heating. The total widths of some partly overlapping reflections first diminish and thereafter increase again on heating, which imply significant changes in the axial ratios. The visual observations and subsequent calculations of unit cell dimensions indicate that the anomalous expansion behavior earlier reported close to the orthorhombic-to-rhombohedral phase transition (40) probably is an artifact introduced by erroneous indexing, probably as a result of the minute line splittings.

PXD, DSC, and calorimetry studies show consistently an increase in the transition temperature, T_d, with t, for both oxidized and reduced samples. High-temperature PXD data were collected for reduced samples, of which some 5 mg were confined in a closed capillary with volume ~1 mm^3. Under such conditions, T_d was found to be 20 K larger for $La_{0.80}Ca_{0.20}CrO_{2.90}$ in a closed capillary than in an open capillary. In the latter case, the sample was oxidized to a large extent prior to the transition, and the value for T_d corresponds to that observed for $La_{0.80}Ca_{0.20}CrO_3$.

The first-order, structural phase transition is manifested in the PXD patterns on the Guinier Simon films by a sudden appearance of line splittings. The close continuity of most reflections throughout the transition region indicates that the volume contraction at the transition (on heating) must be very small. For $LaCrO_3$ the volume jump is $\Delta V/V = -1.4 \times 10^{-3}$, whereas for $t = 0.20$ it is much less and is estimated to be -7×10^{-4} (cf. Figs. 4 and 6). From earlier studies it is known that the jump increases on substituting Cr by Co, $\Delta V/V$ being -4.3×10^{-3} for $LaCr_{0.80}Co_{0.20}O_3$ (41). Momin *et al.* (40) reported that both the orthorhombic (O) to rhombohedral (R) and the rhombohedral to cubic (C) phase transition for $LaCrO_3$ are accompanied by small volume expansions. The present study and Ref. (41) clearly prove a volume contraction for the O to R transition. Whereas Momin *et al.* (40) reported that the R to C transition occurred at 1300 K in air, other studies (42, 43) have provided evidence for a higher transition temperature. On the basis of linear extrapolation of ($\alpha - 60°$) to zero, the R → C transition temperature is estimated to be around 2000 K for $LaCrO_3$ (42, 43). Following the same procedure, 2180, 2080, 2120, and 2260 K were presently obtained for $t =$

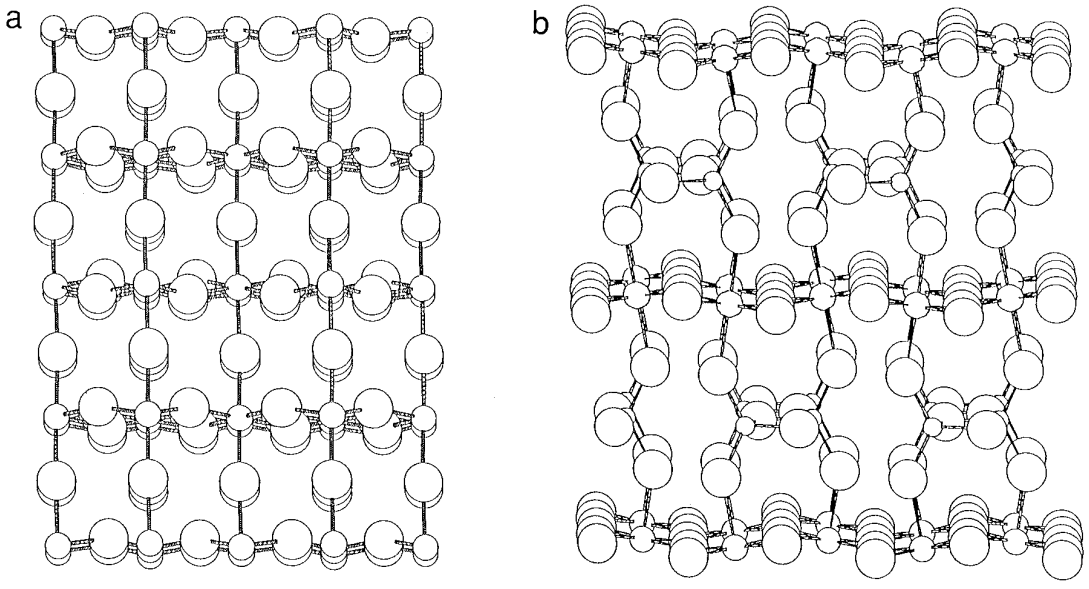

FIG. 3. Comparison of the Brownmillerite- and $GdFeO_3$-type structures. Only transition metal and oxygen atoms are shown. (a) $LaCrO_3$, (b) Brownmillerite.

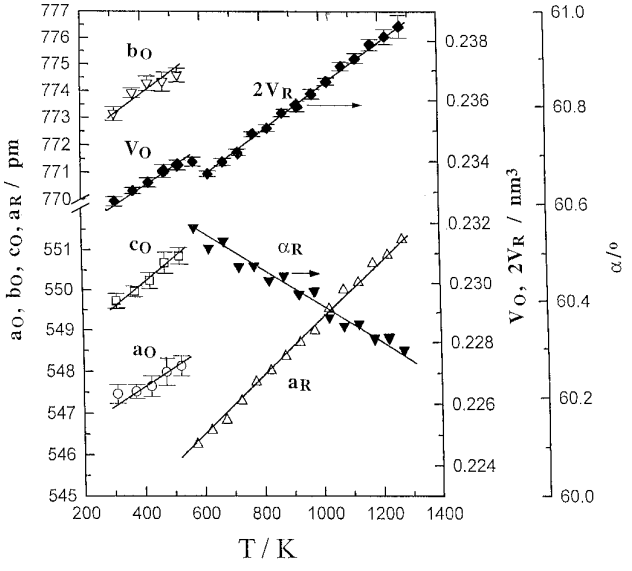

FIG. 4. Temperature dependence of unit cell dimensions for $La_{0.90}Ca_{0.10}CrO_3$.

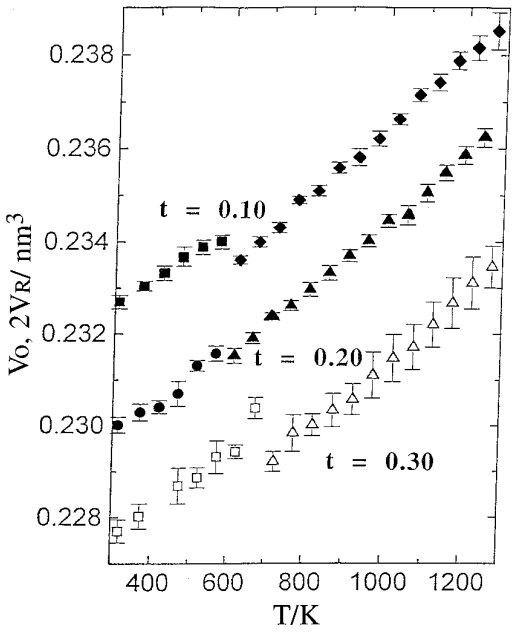

FIG. 6. Variation of unit cell volume, V_O and $2V_R$, for the orthorhombic (O) and rhombohedral (R) modifications of $La_{1-t}Ca_tCrO_{3-\delta}$, $t = 0.10$, 0.20, and 0.30.

0.00, 0.10, 0.20, and 0.30. Note that no experimental data are available for $T > 1300$ K; see Fig. 5. For the quoted composition range, $T_{R\rightarrow C}$ appears to be constant within expected uncertainty.

The temperature dependences of the unit cell dimensions are shown for $La_{0.90}Ca_{0.10}CrO_3$ in Fig. 4. The data are representative for all studied samples with $t \leq 0.30$. Refinements of the orthorhombic unit cell could not be made with sufficient accuracy from the Guinier Simon film data, whereas no problems were encountered in this respect for the rhombohedral unit cell. The results for the orthorhombic regime are deduced from diffractometer data. For $La_{0.80}Ca_{0.20}CrO_{3.00}$, the unit cell volume of the rhombohedral phase just above T_d (614 K) is $V = 231.52 \times 10^6$ pm^3, increasing to 236.24×10^6 pm^3 at 1244 K (Fig. 6). This volume change corresponds to a linear volume expansion coefficient, $\alpha_V = 3.2 \times 10^{-5}$ K^{-1}. As seen from Figs. 4 and 6, α_V is slightly larger for the R than for the O modification. The value for $t = 0.20$ is larger than reported for $LaCrO_3$, for which $\alpha_V = (2.0–2.2) \times 10^{-5}$ K^{-1} (40, 41) for the R modification. There is no major change in expansivity for $La_{1-t}Ca_tCrO_{3-\delta}$ on increasing substitution (Fig. 6). The microscopic picture of rather composition independent expansivity contrasts somewhat with the reported increase of the macroscopic expansion with increasing (Ca, Sr)-substitution (44, 45). The dilatometrically determined linear thermal expansion coefficients (sintered specimens, 3–9% porosity) for $La_{1-t}Ca_tCrO_{3-\delta}$, $(9–10) \times 10^{-6}$ K^{-1} (44, 45), corresponds to $\alpha_V = (2.7–3.0) \times 10^{-6}$ K^{-1}. This value is in fair agreement with the observed expansion of the unit cell volume (see above). The macroscopic expansion of these materials are of importance for high-temperature applications. For $La_{0.80}Ca_{0.20}CrO_{3-\delta}$, a macroscopic expansion $\Delta l/l = 3 \times 10^{-3}$ occurs on reduction, i.e., on lowering $p(O_2)$ from 0.2 and 10^{-15} bar at 1273 K (46). This value for $\Delta l/l$ can be compared with the present unit cell data. At 298 K, the difference in unit cell volume between $La_{0.80}Ca_{0.20}CrO_3$ and

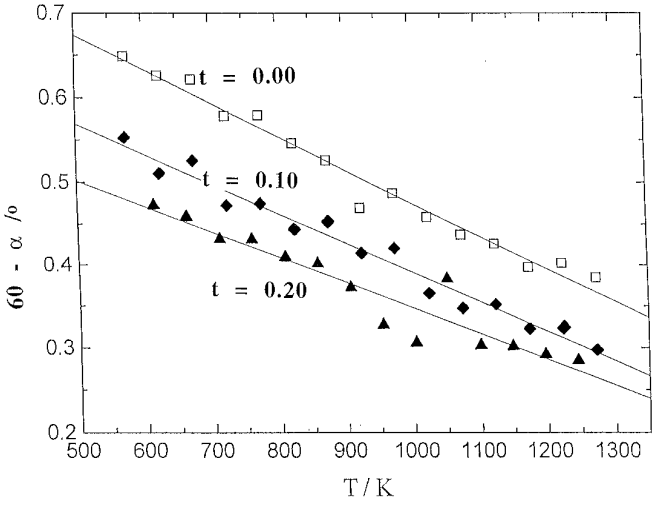

FIG. 5. Deviation of rhombohedral angle, α, from ideal value 60° as function of temperature for $La_{1-t}Ca_tCrO_{3-\delta}$, $t = 0.00$, 0.10, and 0.20. Fully drawn lines represent least squares fits.

TABLE 2
Atomic Coordinates, Temperature Factors, and Oxygen Occupancy for Oxidized Samples of $La_{1-t}Ca_tCrO_3$ from Rietveld Refinements of Powder Neutron Diffraction Data Collected at MURR, USA and at JEEP II, Kjeller, Norway

t	0.00	0.10	0.10	0.20	0.20	0.20[a]	0.30	0.30
T(K)	298	298	12	298	12	12	298	12
Place	MURR	Kjeller	Kjeller	MURR	Kjeller	Kjeller	MURR	Kjeller
$x_{La/Ca}$	0.0188(6)	0.0175(9)	0.0227(6)	0.0185(7)	0.0208(9)	0.006(2)	0.0177(8)	0.025(1)
$z_{La/Ca}$	0.9957(8)	0.997(1)	0.999(1)	0.003(1)	0.997(1)	0.007(2)	0.999(1)	0.996(1)
x_{O1}	0.491(1)	0.493(1)	0.490(1)	0.495(1)	0.491(1)	0.495(3)	0.495(1)	0.493(1)
z_{O1}	0.0661(9)	0.055(2)	0.066(1)	0.060(1)	0.066(2)	0.050(2)	0.056(1)	0.068(1)
x_{O2}	0.2277(7)	0.2286(9)	0.2237(9)	0.2258(7)	0.227(1)	0.236(2)	0.2258(8)	0.223(1)
y_{O2}	0.5347(5)	0.5370(8)	0.5351(6)	0.5338(4)	0.5328(9)	0.539(1)	0.5348(5)	0.531(1)
z_{O2}	0.2263(6)	0.2238(9)	0.2251(9)	0.2264(7)	0.2258(16)	0.242(2)	0.2238(7)	0.224(1)
$B_{La/Ca}$	0.56(8)	−0.4(1)	−0.6(1)	0.8(1)	−0.19(1)	0.0(1)	0.9(1)	0.2(1)
B_{Cr}	0.29(8)	0.7(1)	0.8(1)	0.4(1)	0.9(1)	0.6(2)	0.9(1)	0.3(1)
B_{O1}	0.77(9)	0.9(1)	1.1(2)	1.1(1)	0.4(1)	0.6(1)	1.1(1)	0.7(1)
B_{O2}	0.70(8)	−0.2(1)	−0.2(1)	0.7(1)	0.6(1)	0.8(1)	0.9(1)	−0.3(1)
R_n	8.68	6.89	6.62	6.97	5.43	5.55	7.15	4.31
R_p	15.37	8.40	6.95	13.24	9.34	11.63	13.37	7.99
R_m			3.80		8.50	7.48		9.37

Note. Calculated standard deviations in parentheses. Space group *Pnma*: La/Ca and O(1) in 4(*c*) [x, 1/4, z], Cr in 4(*b*) [0, 0, 1/2], and O(2) in 8(*d*) [x, y, z].

[a] Reduced, oxygen content $\delta = 0.10$ according to TGA analyses. Occupation number n(O1) = 1.00 (fixed), n(O2) = 1.74(4).

$La_{0.80}Ca_{0.20}CrO_{2.90}$ is 2.1×10^6 pm^3, which in average corresponds to $\Delta l/l = 3 \times 10^{-3}$.

3.3. Atomic Arrangement

The powder neutron diffraction data for $t = 0.00$, 0.10, 0.20, and 0.30, at and below room temperature, confirmed that the solid solution is of the pure substitutional type with the orthorhombic $GdFeO_3$-type deformed perovskite atomic arrangement [tilted, slightly deformed octahedra (47)]. From the profile refinements, atomic coordinates, displacement factors, and occupation numbers were derived; see Table 2. An excellent agreement between observed and calculated diffraction patterns were obtained; see representative profiles in Fig. 7. No additional peaks indicative of impurity phases or (partial) defect ordering were observed. There are no significant shifts in the atomic coordinates for $La_{1-t}Ca_tCrO_{3-\delta}$, $0.00 \leq t \leq 0.30$ and $10 \leq T \leq 300$ K. Note that the uncertainties in the Kjeller data are larger than in the MURR data. The displacement factors obtained for the Kjeller data at 12 and 298 K are severely hampered by the small $\sin\Theta/\lambda$ range for the data (≤ 0.42), lack of absorption correction, and strong correlations (between magnetic moments, occupation, and displacement parameters).

The accurate determination of the oxygen content of partly reduced $La_{1-t}Ca_tCrO_{3-\delta}$ is not trivial. Although the uncertainty is quite large, the use of powder neutron diffraction has important benefits compared to methods like total reduction, oxidation to a standard state, iodometry, and electrochemical methods by providing site specific information regarding the oxygen deficiency. The linear $V(t)$ behavior for oxidized samples of $La_{1-t}Ca_tCrO_{3-\delta}$, $0.00 \leq t \leq 0.30$, in Fig. 1, suggests that their oxygen stoichiometries are close to 3.00, which, within one calculated standard deviation, was confirmed by the Rietveld refinements. For the reduced sample $La_{0.80}Ca_{0.20}CrO_{3-\delta}$, the profile refinements of PND data (298 K; Kjeller) gave an overall oxygen stoichiometry of 2.74(4). This fits only reasonable well $\delta = 0.10 \pm 0.01$ as deduced from thermogravimetric reoxidation. Although the refinements are hampered by correlations between displacement factors and occupation numbers, judgement on the basis of reliability factors indicate that the oxygen vacancies are preferably located at the O2 (the 8*d*-) site. When comparing the Brownmillerite- and $GdFeO_3$-type structures (Fig. 3), it is seen that vacancy formation for the O2 atoms may provide tetrahedrally coordinated transition-metal (Cr) atoms. This may indicate that the present structure refinements for oxygen defect $La_{1-t}Ca_tCrO_{3-\delta}$ should be done within the frame of the Brownmillerite-type unit cell rather than within the smaller $GdFeO_3$-type unit cell.

Composition induced changes in the interatomic distances and bonding angles can be evaluated from Table 3. Introduction of the smaller Cr^{IV} at the Cr site shortens the average Cr–O bonds in the deformed CrO_6 octahedron. Application of the bond valence concept (48), selecting the reference Cr^{III}–O bond length as $r_o = 172.4$ pm, facilitates

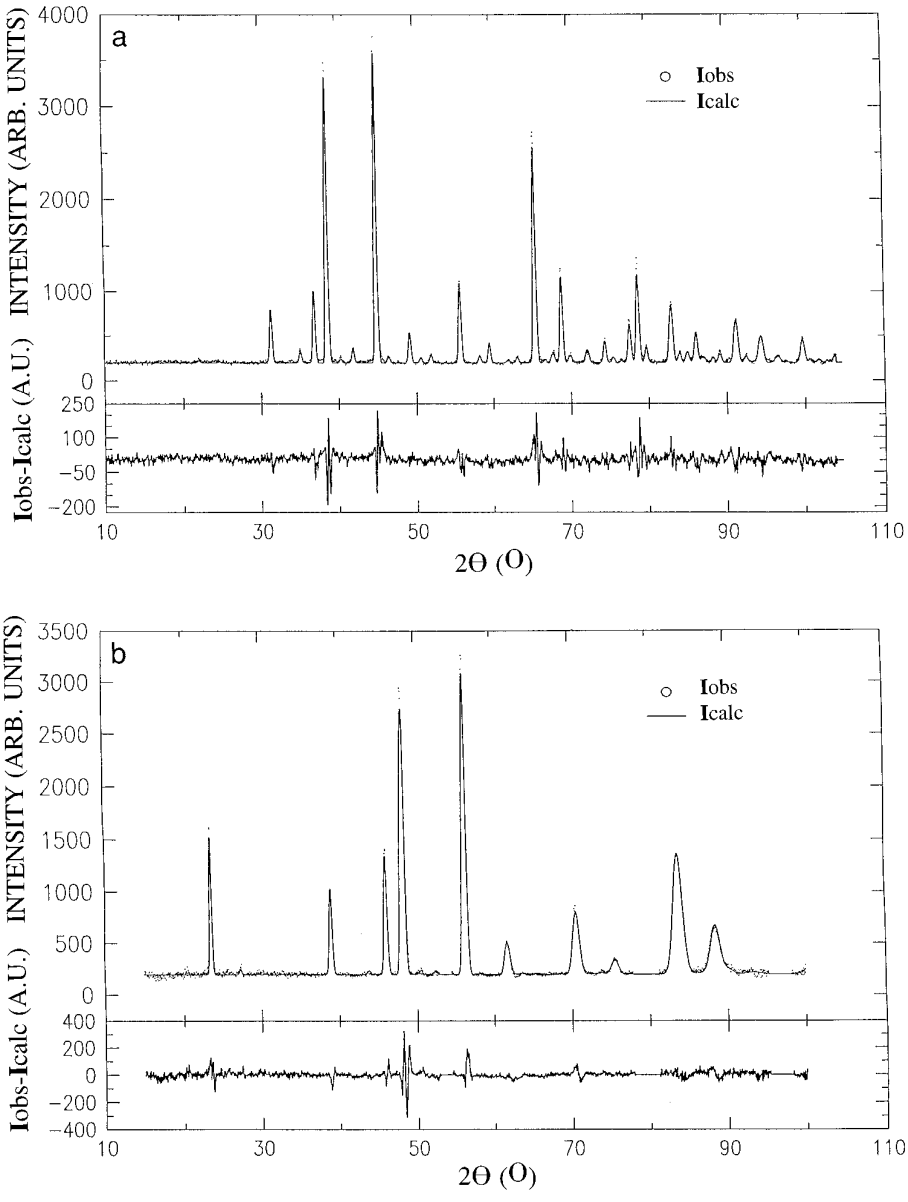

FIG. 7. Observed, calculated, and difference diagrams for powder neutron diffraction data (a) for $La_{0.80}Ca_{0.20}CrO_3$ at 298 K collected at the MURR reactor, U.S.A., λ = 147.66 pm and (b) for $La_{0.80}Ca_{0.20}CrO_{2.90}$ at 12 K collected at the JEEP II reactor, Norway, λ = 182.5 pm.

estimation of the chromium valence. The calculated valence increases from 3.07 to 3.25 between $t = 0.00$ and 0.30, which fits reasonably well the expected variation (from 3.00 and 3.30; assuming no formation of vacancies). Bond strength calculations for lanthanum [r_o = 217.2 pm for La^{III} (48)] are not directly relevant, and the apparent increase in valence from 3.01 for $t = 0.00$ to 3.17 for $t = 0.30$ merely indicates that smaller Ca atoms (r_o = 196.7 pm for Ca^{II}) have entered the La site.

At first sight there are no apparent correlations between crystal structure data and stability of O and R modifications. Whereas the stability of the O modification increases with t, the Cr–O–Cr angles for the corner-sharing octahedra of the orthorhombic phase remain constant around 155°–160° (Table 3) and the deformation in terms of axial ratios actually decrease (toward pseudocubic values). The latter aspect may be understood from empirical correlations between Goldschmidt tolerance factor and structure type, which suggest stabilization of the O modification on reducing *RE* size (presently, the introduction of smaller Ca for La). For *RE* = La (i.e., $LaCrO_3$), the axial ratio parameter ($a/c - 1$) equals −0.007, whereas for *RE* = Dy, Ho, and Lu, these values are 0.049, 0.053, and 0.064. A special aspect of $LaCrO_3$ is hence that the orthorhom-

TABLE 3
Calculated Distances (in pm) and Selected Angles (in Degrees) for Oxidized Samples of $La_{1-t}Ca_tCrO_3$ at 298 K

t =	0.00	0.10	0.20	0.30
		Distances		
La–O1 (1×)	242.2	247.0	240.2	243.2
–O2 (2×)	247.3	245.0	247.5	244.4
–O1 (1×)	262.0	262.3	261.6	261.1
–O2 (2×)	263.3	262.6	264.7	263.5
–O2 (2×)	279.5	280.0	275.0	275.5
–O1 (1×)	291.5	288.3	287.6	286.1
–O1 (1×)	310.3	303.4	308.2	302.8
–O2 (2×)	312.7	313.1	308.7	310.1
Cr–O2 (2×)	196.4	194.9	195.8	194.5
–O1 (2×)	197.5	196.0	195.3	194.9
–O2 (2×)	197.7	198.8	196.1	196.2
		Angles		
Cr–O1–Cr	158.6	162.2	160.7	161.9
Cr–O2–Cr	161.1	160.0	161.2	160.5
v(Cr)	3.07	3.13	3.20	3.25
v(expected)	3.00	3.10	3.20	3.30

Note. Unit cell dimensions determined by PXD and atomic coordinates from PND (MURR) are used. Calculated valence v(Cr) according to the bond valence concept is given for chromium, see text.

bically deformed phase has $a/c < 1$. In this case, enhanced deformation on reducing cation size at the *RE* site will first increase a/c toward one. To evaluate changes in the tolerance factor itself on substitution and/or reduction for $La_{1-t}Ca_tCrO_{3-\delta}$, the average distance ratio d[(La, Ca)–O]/d[Cr–O] should be considered. For the reduced samples, the ratio decreases with increasing substitution level t, whereas for the oxidized samples the shrinkage of the (La, Ca)O_{12} and (Cr^{III}, Cr^{IV})O_6 coordination polyhedra cancel (Table 3). Following the same philosophy, T_d for reduced samples of $La_{1-t}Sr_tCrO_{3-\delta}$ is expected to increase with t (no data available). The observed reduction in T_d for oxidized samples of $La_{1-t}Sr_tCrO_{3-\delta}$ (49) does not necessarily contradict the hypothesis since Sr^{2+} is substantially larger than Ca^{2+}. No data are available for $La_{1-t}Ba_tCrO_{3-\delta}$. On substituting the smaller Co^{III} for Cr^{III}, T_d decreases (41), whereas introduction of the larger Mn^{III} causes an increase in T_d (50).

3.4. Magnetic Properties

The magnetic properties are very sensitive to changes in the oxygen stoichiometry for $La_{1-t}Ca_tCrO_{3-\delta}$ which may involve different amounts of Cr^{III} and Cr^{IV} species. Magnetic susceptibility and neutron diffraction data are presented for oxidized and reduced samples.

The reduced samples are considered first. At low substitution levels, the introduced Ca atoms merely act as a positive chemical pressure on the magnetic sublattice, whereas at higher substitution levels, the substantial oxygen vacancy concentration may influence the Cr–O–Cr interactions, e.g., due to local ordering of defect clusters. The magnetic susceptibility (ZFC) curves for $LaCrO_3$ and $La_{0.80}Ca_{0.20}CrO_{2.90}$ are compared in Fig. 8. Whereas the Néel temperatures are about equal around 290 K, the susceptibility curve for $t = 0.20$ shows a drop around 50 K which probably indicates that additional antiferromagnetic modes are activated or that a spin reorientation occurs. The effect was, however, too small to be determined in the powder neutron diffraction study. The positive chemical pressure exerted by the introduction of smaller *RE* in the series of $RECrO_3$ leads to increased structural deformation and the lowering of T_N, from $T_N = 290$ K for *RE* = La via $T_N = 146$ K for *RE* = Dy to $T_N = 112$ K for *RE* = Lu (51). The volume contraction through the $La_{1-t}Ca_tCrO_3$ solid solution system is large, and the unit cell volume for $t = 0.75$ corresponds roughly to that for $DyCrO_3$.

The magnetic structures for $La_{1-t}Ca_tCrO_{3-\delta}$ were determined on the basis of powder neutron diffraction data (Kjeller). The magnetic Cr atoms occupy the 4*b* sites of the space group *Pnma*. According to representation theory (52), different sets of magnetic modes are possible, for the irreducible representation Γ_{1g} the G_x, C_y, and A_z modes; Γ_{2g} with C_x, G_y, and F_z; Γ_{3g} with F_x, A_y, and C_z; and finally Γ_{4g} with A_x, F_y, and G_z. The magnetic structure of $LaCrO_3$ was confirmed as a G_x mode (belonging to Γ_{1g}) with the six surrounding chromium atoms antiferromagnetically coupled. Also for $La_{0.80}Ca_{0.20}CrO_{2.90}$, the G_x mode was the only one present. For $RECrO_3$ in general, *G*-type ordering (separate or combined, G_x and G_y) is most common. The small A_z component listed in Table 4 for $LaCrO_3$ is not considered significant.

For the oxidized samples, the magnetic susceptibility behavior (under ZFC conditions) is strongly affected by substitution (Fig. 8b). The ordering temperature, T_N, decreases from 290 K for $LaCrO_3$ to 190 K for $t = 0.30$. Measurements for the partly oxidized $t = 0.75$ samples gave $T_N = 80 \pm 5$ K. These observations fall fairly well in line with the reported antiferromagnetic order for $CaCrO_3$ below $T_N = 90$ K (52).

$CaCrO_3$ is reported to show parasitic ferromagnetism ($\sigma = 0.295$ emu $\cdot$ g^{-1} at 4.2 K) below the first-order transition at 90 K (53). Such behavior was observed for all oxidized samples of the $La_{1-t}Ca_tCrO_{3-\delta}$ solid solution. This is illustrated by the recorded magnetic susceptibility under field cooled (FC) conditions in Fig. 8c. The spontaneous magnetization vanishes on heating in zero field at the same temperature, T_N, as found for the ZFC samples. For $t = 0.20$ the spontaneous magnetization at 5 K is 0.26 emu $\cdot$ g^{-1}, i.e., approximately as for $CaCrO_3$.

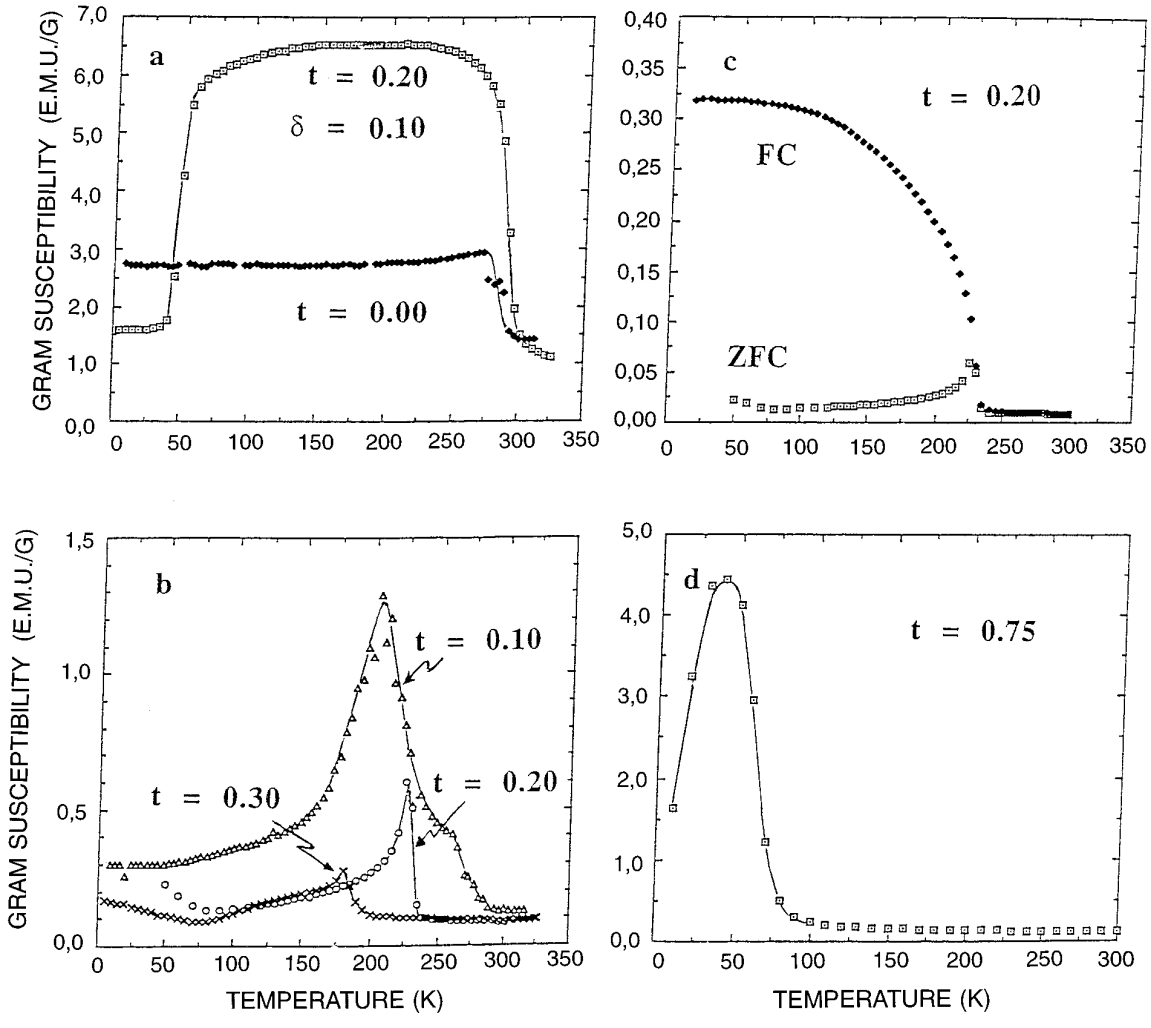

FIG. 8. Magnetic susceptibility (ZFC) for $La_{1-t}Ca_tCrO_{3-\delta}$ between 5 and 300 K; (a) $t = 0.00$ and reduced $t = 0.20$ ($\delta = 0.10$), (b) oxidized samples $t = 0.10$, 0.20, and 0.30 (c) $t = 0.20$ (oxidized) at zero field cooling (ZFC) and field cooling (FC; 1 Oe) conditions and (d) $t = 0.75$. Fully drawn lines guide the eye.

TABLE 4
Refined Magnetic Moments for $La_{1-t}Ca_tCrO_{3-\delta}$ from Powder Neutron Diffraction Data at 12 K, Kjeller[b]

	t				
Mode	0.00	0.10 (ox)[a]	0.20 (ox)	0.20 (red)[a]	0.30 (ox)
G_x	2.49(2)[b]	2.77(3)	2.51(3)	2.52(3)	2.03(3)
C_y	0[c]	0	0	0	0
A_z	0.12(3)[d]	0.28(12)	0.60(8)	0	0.61(8)

[a] ox = oxidized, red = reduced.
[b] Calculated standard deviations in parentheses.
[c] Numbers given as zero indicate that the refined value is zero within calculated standard deviation.
[d] See text.

The G_x mode dominates also for the oxidized samples. The additional magnetic scattering contributions to certain Bragg reflections is evident from the diffraction profiles in Fig. 7b. In the Rietveld refinements, the possible coexistence of the additional modes, C_y and A_z, transforming according to the same irreducible representation (Γ_{1g}) was considered. The results show that increasing calcium content (and hence Cr^{IV} content) induces a small A_z component. Derived magnetic moments are given in Table 4. The magnetic structures (G_x and G_xA_z) are sketched in Fig. 9. For the oxidized samples with $0.10 \leq t \leq 0.30$, the ordered magnetic moment at 10 K decreases in accordance with Cr^{III} (d^3) being partially replaced by Cr^{IV} (d^2). The field induced parasitic ferromagnetism (see above) must involve other representations than Γ_{1g}, whereby the magnetic symmetry is lowered to the monoclinic system.

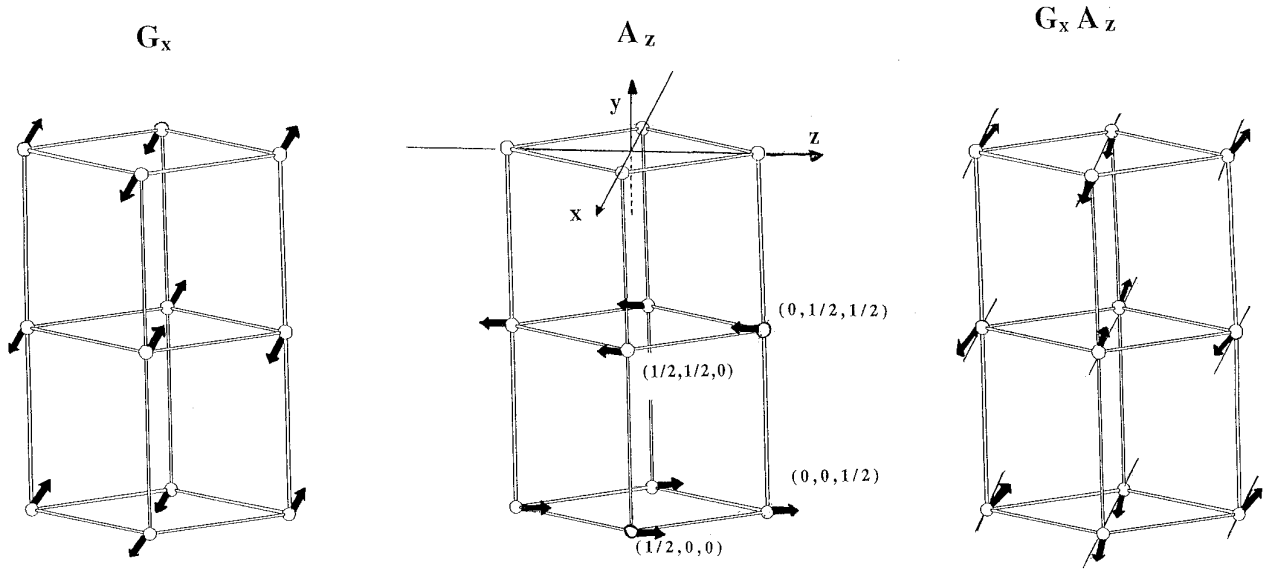

FIG. 9. Magnetic structure for (La, Ca)CrO_3 at 12 K, showing the pure G_x mode (left; $LaCrO_3$), the pure A_z mode (middle), and the G_xA_z mode (right, $La_{0.70}Ca_{0.30}CrO_{3.00}$).

In the PND study, the magnetic ordering temperatures were determined from the integrated intensities of selected reflections with, entire or large, magnetic intensity contributions (cf. Fig. 7b). The temperature dependence of $(I_{011} + I_{110})$ is shown in Fig. 10. The magnetic and structural phase diagram for $La_{1-t}Ca_tCrO_3$ is sketched in Fig. 11 for oxidized samples. [For reduced samples, T_d would be somewhat higher (20 K higher for $t = 0.20$) whereas T_N would stay roughly constant at 290 K for $t \leq 0.20$.]

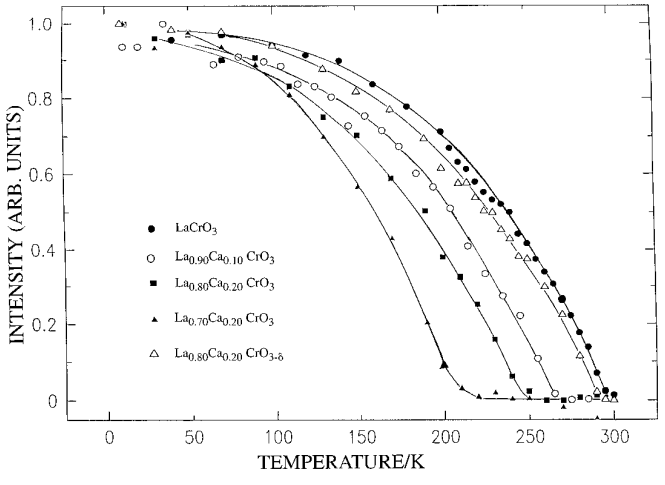

FIG. 10. Integrated intensities for the overlapping 110 and 011 reflections (at $2\Theta = 23.5°$, $\lambda = 182.5$ pm) versus temperature for $La_{1-t}Ca_tCrO_{3-\delta}$; $t = 0.00$, 0.10, 0.20, and 0.30 for $\delta = 0.00$ and $t = 0.20$ for $\delta = 0.10$. Fully drawn lines guide the eye.

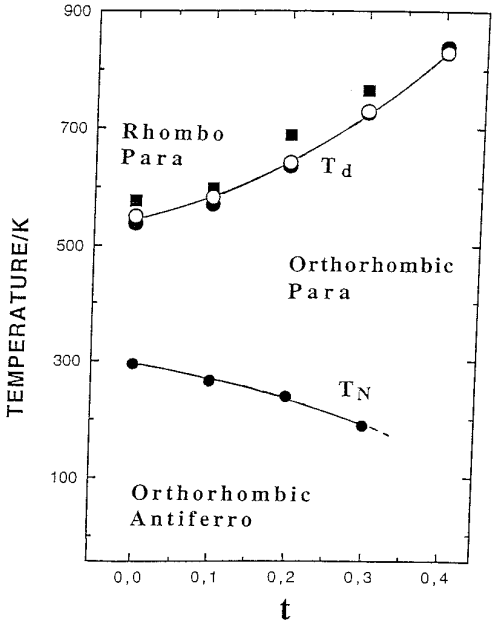

FIG. 11. Structural and magnetic phase diagram for oxidized samples of $La_{1-t}Ca_tCrO_3$ for $0.00 \leq t \leq 0.30$ and $5 \leq T \leq 900$ K.

ACKNOWLEDGMENTS

Dr. Ron Berliner is sincerely thanked for assistance with powder neutron diffraction experiments at MURR. This work has obtained support from the Research Council of Norway.

REFERENCES

1. D. B. Meadowcroft, *Br. J. Appl. Phys.* (*J. Phys. D*) **2,** 1225 (1969).
2. W. Baugal, W. Kunn, H. Kleischmager, and F. J. Rohr, *J. Power Sources* **1,** 203 (1976/77).
3. W. Feduska and A. O. Isenberg, *J. Power Sources* **10,** 89 (1983).
4. B. K. Flandermayer, J. T. Dusek, P. E. Blackburn, D. W. Dees, C. C. McPheeters, and R. B. Poeppel, *in* "Abstracts from Fuel Cell Seminar, Tucson, AZ, 1986," p. 68. Courtesy Associated Inc., Washington, 1986.
5. W. Shafer and R. Schmidberger, *in* "High Tech Ceramics" (P. Vincentini, Ed.). Elsevier, Amsterdam, 1987.
6. D. P. Karim, and A. T. Aldred, *Phys. Rev. B* **20,** 2255 (1979).
7. K. Gaur, S. C. Verma, and H. B. Lal, *J. Mater. Sci.* **23,** 1725 (1988).
8. A. K. Tripathi and H. B. Lal, *Mater. Res. Bull.* **15,** 233 (1980).
9. J. Mizusaki, S. Yamauchi, K. Fueki, and A. Ishikawa, *Solid State Ionics* **12,** 119 (1984).
10. B. F. Flandermayer, M. M. Nasrallah, D. M. Spalin, and H. U. Anderson, *High Temp. Sci.* **20,** 259 (1985).
11. R. Berjoan, C. Romand, and J.-P. Coutures, *High Temp. Sci.* **13,** 173 (1980).
12. C. P. Khattak and D. E. Cox, *Mater. Res. Bull.* **12,** 463 (1977).
13. K. P. Bansal, S. Kumari, B. K. Das, and G. C. Dain, *J. Mater. Sci.* **18,** 2095 (1983).
14. I. Yasuda and T. Hikita, *J. Electrochem. Soc.* **141,** 1268 (1994).
15. L. Groupp and H. U. Anderson, *J. Am. Ceram. Soc.* **59,** 449 (1976).
16. K. P. Bansal, S. Kumari, B. K. Das, and G. C. Jain, *Trans. J. Br. Ceram. Soc.* **80,** 215 (1981).
17. S. Song, M. Yoshimura, and S. Somiya, *J. Mater. Sci. Soc. Jpn.* **19,** 49 (1982).
18. M. P. Pechini, U.S. Patent No. 3,330,697 (1967).
19. JCPDS, Powder Diffraction File No. 5-565.
20. N. O. Ersson, Program CELLKANT, Department of Chemistry, University of Uppsala, Uppsala, Sweden, 1981.
21. K. Yvon, W. Jeitschko, and E. Parthé, *J. Appl. Crystallogr.* **10,** 73 (1977).
22. J. Spreadborough and J. W. Christian, *J. Sci. Instrum.* **36,** 116 (1959).
23. C. W. Tompson, D. F. R. Mildner, M. Mehregany, J. Sudol, R. Berliner, and W. B. Yelon, *J. Appl. Crystallogr.* **17,** 385 (1984); R. Berliner, K. McCollough, and J. Hilker Draper, Research Reactor Facility, University of Missouri, Columbia, MO, 1989.
24. H. M. Rietveld, *J. Appl. Crystallogr.* **2,** 65 (1969).
25. A. W. Hewat, The Rietveld Computer Program for the Profile Refinement of Neutron Diffraction Powder Patterns Modified for Anisotropic Thermal Vibrations, UKAERE Harwell Report RRL 73/897 1973.
26. G. S. Pawley, *J. Appl. Crystallogr.* **13,** 630 (1980).
27. G. S. Pawley, *J. Appl. Crystallogr.* **14,** 357 (1961).
28. V. F. Sears, *Neutron News,* **3** (3) (1992).
29. R. E. Watson and A. J. Freeman, *Acta Crystallogr.* **14,** 27 (1961).
30. R. Berjoan, *Rev. Int. Hautes Temp. Refract.* **13,** 119 (1976).
31. J. B. Goodenough, J. M. Longo, and J. A. Kafalas, *Mater. Res. Bull.* **3,** 471 (1968).
32. I. Kontoulis and B. C. H. Steele, *J. Eur. Ceram. Soc.* **9,** 459 (1992).
33. R. Glenne, J. A. Horst, S. Jørgensen, T. Norby, and M. Seiersten, *Surf. Interface Anal.* **22,** 275 (1994).
34. J. D. Carter, V. Sprenkle, M. M. Nasrallah, and H. U. Anderson, *Proc. 3. Int. Symp. Solid Oxide Fuel Cells, Electrochem. Soc. Proc.* **93-4,** 344 (1993).
35. P. Villars and L. D. Calvert, "Pearson's Handbook of Crystallographic Data for Intermetallic Phases." Am. Soc. for Metals, Metals Park, Ohio, 1985.
36. H. Fjellvåg, O. H. Hansteen, B. Gilbu, A. Olafsen, N. Sakai, and H. Seim, Thermochim. Acta **256,** 75 (1995).
37. J. A. M. van Roosmalen and E. H. P. Cordfunke, *J. Solid State Chem.* **93,** 212 (1991).
38. A. A. Colville and S. Geller, *Acta Crystallogr. Sect. B* **27,** 2311 (1971).
39. J. M. Gonzales-Calbet, J. Ramirez, and M. Vallet-Regi, *J. Less Comm. Met.* **157,** 271 (1990).
40. A. C. Momin, E. B. Mirza, and M. D. Mathews, *J. Mater. Sci. Lett.* **10,** 1246 (1991).
41. B. G. Tilset, H. Fjellvåg, and A. Kjekshus, *J. Solid State Chem.* **119,** 271 (1995).
42. S. Geller and P. M. Raccah, *Phys. Rev. B* **2,** 1167 (1970).
43. J.-P. Traverse and R. Berjoan, *C. R. Acad. Sci. Paris C* **276,** 1167 (1973).
44. S. P. Tolochko, I. F. Kononyuk, V. A. Lyutsko, and Yu. G. Zonov, *Izv. Akad. Nauk SSSR Neorg. Mater.* **23,** 1520 (1987).
45. N. Sakai, T. Kawada, H. Yokokawa, M. Dokiya, and T. Iwata, *Solid State Ionics* **40/41,** 394 (1990).
46. W. Schafer and R. Schmidberger, *High Tech. Ceram.* 1737 (1987).
47. A. M. Glazer, *Acta Crystallogr. Sect. B* **28,** 3384 (1972).
48. N. E. Brese and M. O'Keeffe, *Acta Crystallogr. Sect. B* **47,** 192 (1991).
49. P. S. Devi and M. S. Rao, *J. Solid State Chem.* **98,** 237 (1992).
50. S. A. Howard, J.-K. Yau, and H. U. Anderson, *J. Am. Chem. Soc.* **75,** 1685 (1991).
51. A. Olés, A., F. Kajzar, M. Kucab, and W. Sikora, "Magnetic Structures Determined by Neutron Diffraction." Polska Akademia Nauk, Warzawa, Krakow, 1976.
52. E. F. Bertaut, *Acta Crystallogr. Sect. A* **24,** 217 (1968).
53. J. F. Weiher, B. L. Chamberland, and J. L. Gillson, *J. Solid State Chem.* **3,** 529 (1971).